

## A general and facile synthesis strategy towards highly porous carbons: carbonization of organic salts†

Marta Sevilla and Antonio B. Fuertes\*

Cite this: *J. Mater. Chem. A*, 2013, **1**, 13738Received 9th August 2013  
Accepted 3rd October 2013

DOI: 10.1039/c3ta13149a

www.rsc.org/MaterialsA

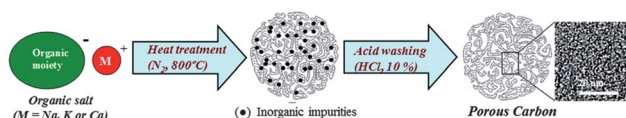
Highly porous carbons with different textural properties were obtained in only one step by means of simple heat-treatment of organic salts of Na, K or Ca. The pore characteristics were tuned from a microporous to a mesoporous carbon by simply choosing the appropriate organic salt.

The development of novel procedures for the synthesis of porous carbons has generated renewed interest due to the importance these materials have for applications related to energy storage, catalysis, gas storage, *etc.*<sup>1</sup> Among the procedures used to generate porosity in carbon materials, chemical activation has attracted a great deal of attention because it is able to produce porous carbons with extremely large surface areas, high pore volumes and porosity made up of micropores (<2 nm) and small mesopores (~2–5 nm).<sup>2</sup> These textural properties make such carbons particularly suitable for use as electrodes in supercapacitors,<sup>3</sup> Li-ion battery anodes,<sup>4</sup> CO<sub>2</sub> adsorbents<sup>5</sup> or hydrogen storage carriers.<sup>6</sup> Chemical activation consists of heat treatment under an inert atmosphere of a mixture of a carbonaceous material and certain chemical compounds such as alkali hydroxides (*i.e.* KOH and NaOH), phosphoric acid, ZnCl<sub>2</sub>, *etc.*<sup>7</sup> These compounds react with the carbon framework which is partially etched, thereby generating a well-developed micro-mesoporous network. However, this process suffers from several drawbacks, such as the need for a large excess of corrosive chemical compounds, special equipment and rigorous washing conditions. For these reasons, the preparation of highly porous carbons by a facile and sustainable method is still a challenge to be overcome. Recently reports have appeared showing the production of porous carbons by the carbonization of organic salts such as ethylenediamine

tetraacetic acid disodium magnesium<sup>8</sup> or alkali chloroacetates.<sup>9</sup> However, these studies based on the use of rare organic salts do not provide a clear image either of the general scope of the procedure or of the activation mechanism responsible for the generation of porosity.

Herein, we present a general synthesis route for the production of porous carbons. It is based on the use of common organic salts of Na, K or Ca as precursors. These compounds combine a carbon precursor (*i.e.* the organic moiety) and certain elements which can generate during heat-treatment inorganic species capable of operating as activating agents. The alkali salts were selected taking into account that several inorganic compounds of K and Na are well-known chemical activating agents, and the calcium compounds give rise to CaO nanoparticles capable of generating mesopores. Furthermore, the uniform dispersion of such elements within the organic matrix at a molecular level suggests that the activation process will be effective in spite of the relatively low inorganic species content. In this way, highly porous carbons can be produced in only one simple step, avoiding the use of large amounts of corrosive chemical agents. In order to verify this hypothesis, we selected a variety of organic salts of Na, K, and Ca; *i.e.* gluconates, alginate and citrates. The synthesis procedure is illustrated in Scheme 1. Basically, it consists in the heat treatment of organic salts up to 800 °C. The carbonized-activated product is then purified by washing with diluted hydrochloric acid to remove the inorganic impurities. Details of the experimental procedure are provided in the ESI.†

The SEM images shown in Fig. 1 reveal that, depending on the organic salt used, the synthesised carbons exhibit a variety



**Scheme 1** Illustration of the synthesis procedure for obtaining porous carbons by carbonization of organic salts.

Instituto Nacional del Carbón (CSIC), P. O. Box 73, 33080, Oviedo, Spain. E-mail: abefu@incar.csic.es; Fax: +34 985 297662; Tel: +34 985 119090

† Electronic supplementary information (ESI) available: Experimental section, nitrogen sorption isotherms and pore size distributions, and XRD patterns. See DOI: 10.1039/c3ta13149a

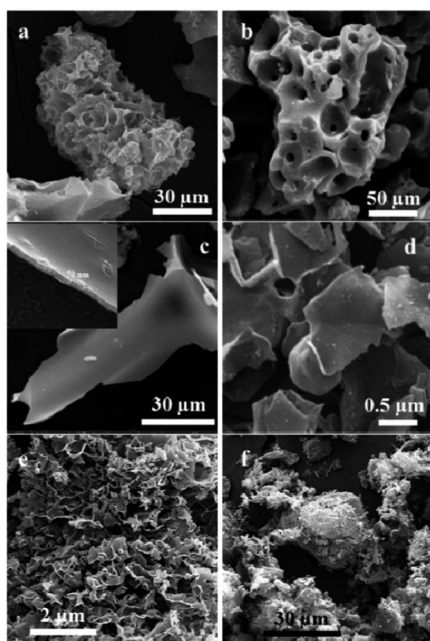


**Fig. 1** SEM images of carbons produced by the carbonization of organic salts at 800 °C: (a) C-NaA, (b) C-KG, (c) C-NaG (inset: magnified image of the carbon nanosheet thickness), (d) C-KC, (e) C-NaC and (f) C-CaC.

of morphologies: (a) irregular particles (samples from calcium salts: C-CaG, C-CaA and C-CaC), (b) vesiculated particles (C-KG and -NaA), (c) sponge-like particles (C-NaC) and (d) nanosheets (C-NaG and C-KC). The codes of the carbon samples are shown in Table 1. Interestingly, large carbon nanosheets (>100 μm length and <100 nm thickness) are obtained from sodium gluconate (Fig. 1c) and small carbon nanosheets (<2 μm length) can be produced from potassium citrate (Fig. 1d). The carbon nanosheets are of special interest given that short diffusional paths considerably diminish mass transfer resistance, which is important in the case of supercapacitors due to the enhancement of the ion-transport kinetics.<sup>10</sup>

The textural parameters of the synthesised carbons are listed in Table 1. These results show that the porous carbons have large Brunauer–Emmett–Teller (BET) surface areas, whose

values vary over a wide range, between 650 m<sup>2</sup> g<sup>−1</sup> in the case of C-NaC carbon and 1960 m<sup>2</sup> g<sup>−1</sup> in the case of C-KC sample. Similarly, the pore volumes vary from 0.54 cm<sup>3</sup> g<sup>−1</sup> for C-CaA to 2.6 cm<sup>3</sup> g<sup>−1</sup> for C-CaC. These data clearly confirm our hypothesis and show that an effective activation process occurred during the heat-treatment of the organic salts. Furthermore, the results listed in Table 1 reveal that the textural properties and the characteristics of the pore network depend heavily on the type of organic salt. The N<sub>2</sub> sorption isotherms and the mesopore size distributions for four representative carbons are depicted in Fig. 2, while the sorption isotherms for the rest of carbons are shown in Fig. S1 (ESI†). The mesopore size distribution was determined by means of the Kruk–Jaroniec–Sayari method applied to the N<sub>2</sub> adsorption branch.<sup>11</sup> The pore size distributions for the micro–mesopore range (0.5–5 nm)

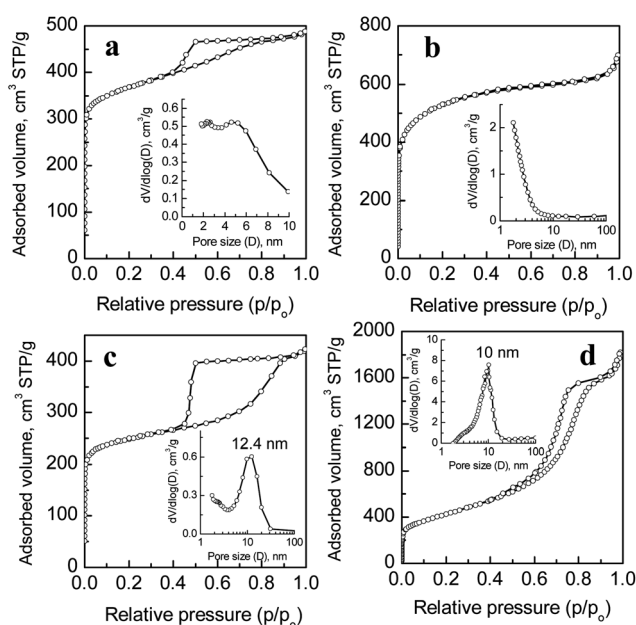


**Fig. 2** Nitrogen sorption isotherms and mesopore size distributions (insets) of carbons produced by heat treatment at 800 °C of: (a) potassium gluconate (C-KG), (b) potassium citrate (C-KC), (c) sodium gluconate (C-NaG) and (d) calcium citrate (C-CaC).

**Table 1** Textural properties of the porous carbons obtained by the heat-treatment of various organic salts at 800 °C

Sample code	Organic salt	$S_{\text{BET}}$ (m <sup>2</sup> g <sup>−1</sup> )	$V_p^a$ (cm <sup>3</sup> g <sup>−1</sup> )	$V_{\text{micro}}^b$ (cm <sup>3</sup> g <sup>−1</sup> )	$V_{\text{meso}}^c$ (cm <sup>3</sup> g <sup>−1</sup> )
C-NaG	Sodium gluconate	960	0.65	0.31 (0.9)	0.34
C-KG	Potassium gluconate	1410	0.76	0.57 (0.9)	0.19
C-CaG	Calcium gluconate	790	0.69	0.29 (0.8)	0.40
C-NaC	Sodium citrate	650	0.40	0.24 (1.3)	0.16
C-KC	Potassium citrate	1960	1.08	0.85 (1.4)	0.23
C-CaC	Calcium citrate	1510	2.6	0.07	2.5
C-NaA	Sodium alginate	1250	0.63	0.50 (1.1)	0.13
C-CaA	Calcium alginate	830	0.54	0.35 (0.9)	0.19

<sup>a</sup> Pore volume at  $p/p_0 \sim 0.95$ . <sup>b</sup> Micropore volume determined by the  $t$ -plot technique; the mean micropore size deduced by applying the Dubinin–Radushkevich (D–R) method to the N<sub>2</sub> adsorption branch, is indicated in brackets. <sup>c</sup> Mesopore volume obtained by the difference between the pore volume ( $V_p$ ) and micropore volume ( $V_{\text{micro}}$ ).



obtained by the QSDFT method are displayed in Fig. S2.† For the carbons derived from potassium salts it was observed that the porosity is basically made up of micropores together with a small fraction of mesopores. Thus, the micropore volumes for these samples constitute around 75% of the total pore volume (see Table 1), the mean micropore sizes being in the order of 0.9 nm (C-KG) and 1.4 nm (C-KC) as deduced by the D-R method (see Table 1). The textural properties of the C-KC sample have a special relevance. Thus, this carbon exhibits a very high BET surface area of  $1960 \text{ m}^2 \text{ g}^{-1}$ , a large pore volume of  $1.08 \text{ cm}^3 \text{ g}^{-1}$  and a porosity made up of supermicropores and small mesopores, as illustrated by the pore size distribution shown in Fig. S2d.† These textural properties are similar to those of porous carbons produced by chemical activation with KOH.<sup>12</sup> On the other hand, the carbons obtained by the carbonization of sodium gluconate (C-NaG) and calcium citrate (C-CaC) exhibit a porosity made up essentially of mesopores (see Table 1 and Fig. 2c and d). Thus, the porosity of C-NaG carbon nanosheets (see Fig. 1c) is made up of uniform mesopores of around 12 nm with a mesopore volume of  $0.34 \text{ cm}^3 \text{ g}^{-1}$ . These mesopores have a cage-like structure, as suggested by the hysteresis loop (Fig. 1c) and evidenced by the TEM image in Fig. 3a. This image illustrates the structure of these mesopores which consists of spherical nanovoids interconnected by narrow micropores. Interestingly, the C-CaC carbon exhibits exceptional textural properties, which are typical of templated mesoporous carbons produced by nanocasting techniques.<sup>13</sup> Thus, it has a porosity made up exclusively of uniform mesopores of  $\sim 10 \text{ nm}$ , a BET surface area of  $1510 \text{ m}^2 \text{ g}^{-1}$  and a pore volume of  $2.6 \text{ cm}^3 \text{ g}^{-1}$ . The TEM image in Fig. 3b illustrates the mesoporous structure of the C-CaC sample, which consists of randomly distributed mesopores.

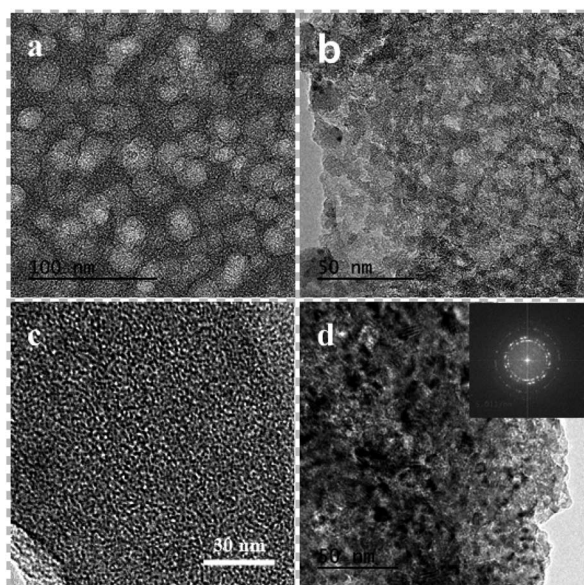


**Fig. 3** TEM images of the samples: (a) C-NaG, (b) C-CaC, (c) C-KC and (d) calcium citrate heat-treated at  $800^\circ\text{C}$  (the black regions correspond to CaO nanoparticles. Inset: SAED pattern corresponding to the area covered by this image).

The thermal treatment of alkali organic salts shows certain analogies with the reaction between the inorganic compounds (*i.e.* KOH and NaOH) and the carbon precursors during the chemical activation process.<sup>14</sup> At relatively low temperatures (*i.e.*  $500\text{--}650^\circ\text{C}$ ), the formation of alkali carbonates (*i.e.*  $\text{K}_2\text{CO}_3$  or  $\text{Na}_2\text{CO}_3$ ) takes place, as evidenced by the XRD patterns shown in Fig. S3 (ESI†). At higher temperatures, these carbonates decompose ( $\text{M}_2\text{CO}_3 \rightarrow \text{M}_2\text{O} + \text{CO}_2$ ,  $\text{M} = \text{Na}$  or  $\text{K}$ ) and the evolved  $\text{CO}_2$  reacts with carbon ( $\text{C} + \text{CO}_2 \rightarrow 2 \text{CO}$ ), generating thereby a certain microporosity. Simultaneously, metallic sodium or potassium is produced by the reduction of the alkali oxides by carbon ( $\text{M}_2\text{O} + \text{C} \rightarrow 2\text{M} + \text{CO}$ ). The presence of deposits of these alkali metals was observed in the cool parts of the carbonization reactor. These alkali metals play a crucial role in the generation of additional porosity because their vapours are intercalated between the graphene layers, causing swelling and disruption of the carbon microstructure. These reactions lead to the formation of highly porous carbons such as C-KC whose microporous structure is illustrated in the TEM image in Fig. 3c. The reaction mechanism for the calcium organic salts is slightly different. In this case, the formation of  $\text{CaCO}_3$  at relatively low temperatures takes place, as revealed by the XRD pattern obtained for the calcium citrate treated at  $500^\circ\text{C}$  (Fig. S3c†). At higher temperatures, the carbonate decomposes ( $\text{CaCO}_3 \rightarrow \text{CaO} + \text{CO}_2$ ) and the  $\text{CO}_2$  released generates certain porosity *via* the gasification reaction of carbon. However, unlike the alkali oxides, the CaO is not reduced by the carbon. Thus, the XRD pattern obtained for the calcium citrate treated at  $800^\circ\text{C}$  reveals the presence of CaO nanoparticles with a size of around  $11 \text{ nm}$ , as can be deduced by applying the Scherrer equation to the (200) peak (see Fig. S3d†). These CaO nanoparticles are located inside the carbonaceous matrix as can be deduced from the TEM image (Fig. 3d) and the selected area electron diffraction pattern (inset in Fig. 3d). It is clear that the CaO nanoparticles act as a hard template, the mesopores of the C-NaC sample being generated once the nanoparticles have been removed. This is confirmed by the fact that the size of CaO nanoparticles ( $11 \text{ nm}$ ) is close to the diameter of the mesopores of the C-CaC sample ( $\sim 10 \text{ nm}$ ) (see Fig. 2d).

In summary, we have presented a novel, general and facile one-step synthesis strategy for producing porous carbons. The procedure only requires the heat-treatment of an organic salt of Na, K or Ca up to a temperature of around  $800^\circ\text{C}$ . The porous carbons thus produced have BET surface areas of up to  $1960 \text{ m}^2 \text{ g}^{-1}$  and pore volumes of up to  $2.6 \text{ cm}^3 \text{ g}^{-1}$ . Interestingly, the pore characteristics of the synthesised carbons can be modulated by selecting the appropriate organic salt. In this way, carbons with a porosity made up exclusively of micropores or mesopores can be easily synthesised. In addition, it was found that certain organic salts (*i.e.* sodium gluconate or potassium citrate) give rise to porous carbons with a nanosheet morphology, which, in the case of sodium gluconate, exhibits very large aspect ratios (length/thickness  $> 10^3$ ). The synthesis strategy presented here has been demonstrated for three types of organic salts (*i.e.* gluconates, citrates and alginates), but it could be further extended to other types of organic salts of Na, K or Ca. The variety of pore and morphological characteristics of these carbons clearly suggests





that several types of these materials would be suitable for use as electrodes in supercapacitors, ion-Li anodes, high performance adsorbents or catalytic supports.

This research work was supported by Spanish MINECO (MAT2012-31651). M.S. acknowledges the award of the *Ramón y Cajal* contract.

## Notes and references

- (a) Y. Zhai, Y. Dou, D. Y. Zhao, P. F. Fulvio, R. T. Mayes and S. Dai, *Adv. Mater.*, 2011, **23**, 4828; (b) N. A. Kaskhedikar and J. Maier, *Adv. Mater.*, 2009, **21**, 2664; (c) M. Jorda-Beneyto, F. Suarez-Garcia, D. Lozano-Castello, D. Cazorla-Amoros and A. Linares-Solano, *Carbon*, 2007, **45**, 293; (d) V. Calvino, A. J. Lopez, C. J. Duran and R. M. Martin, *Catal. Rev.: Sci. Eng.*, 2010, **52**, 325.
- (a) M. Molina-Sabio and F. Rodriguez-Reinoso, *Colloids Surf., A*, 2004, **241**, 15; (b) D. Lozano-Castello, J. M. Calo, D. Cazorla-Amoros and A. Linares-Solano, *Carbon*, 2007, **45**, 2529; (c) J. A. Macia-Agullo, B. C. Moore, D. Cazorla-Amoros and A. Linares-Solano, *Carbon*, 2004, **42**, 1367.
- L. Wei, M. Sevilla, A. B. Fuertes, R. Mokaya and G. Yushin, *Adv. Energy Mater.*, 2011, **1**, 356.
- L. Qie, W.-M. Chen, Z.-H. Wang, Q.-G. Shao, X. Li and L.-X. Yuan, *Adv. Mater.*, 2012, **24**, 2047.
- M. Sevilla, P. Valle-Vigón and A. B. Fuertes, *Adv. Funct. Mater.*, 2011, **21**, 2781.
- M. Sevilla, A. B. Fuertes and R. Mokaya, *Energy Environ. Sci.*, 2011, **4**, 1400.
- (a) S. J. Allen and L. Whitten, *Dev. Chem. Eng. Miner. Process.*, 1998, **6**, 231; (b) M. A. Lillo-Rodenas, J. Juan-Juan, D. Cazorla-Amoros and A. Linares-Solano, *Carbon*, 2004, **42**, 1371; (c) Y. Nakagawa, M. Molina-Sabio and F. Rodriguez-Reinoso, *Microporous Mesoporous Mater.*, 2007, **103**, 29.
- (a) B. Xu, D. Zheng, M. Jia, G. Cao and Y. Yang, *Electrochim. Acta*, 2013, **98**, 176; (b) B. Xu, H. Duan, M. Chu, G. Cao and Y. Yang, *J. Mater. Chem. A*, 2013, **1**, 4565.
- J. D. Atkinson and M. J. Rood, *Microporous Mesoporous Mater.*, 2012, **160**, 174.
- (a) Z. Fan, Y. Liu, J. Yan, G. Ning, Q. Wang and F. Wei, *Adv. Energy Mater.*, 2012, **2**, 419; (b) B. Jang, M. Park, O. B. Chae, S. Park and T. Hyeon, *J. Am. Chem. Soc.*, 2012, **134**, 15010; (c) M. Liu, Y. Yan, L. Zhang and C. Wang, *J. Mater. Chem.*, 2012, **22**, 11458.
- M. Kruk, M. Jaroniec and A. Sayari, *Langmuir*, 1997, **13**, 6267.
- M. Sevilla and A. B. Fuertes, *Energy Environ. Sci.*, 2011, **4**, 1765.
- (a) J. Lee, J. Kim and T. Hyeon, *Adv. Mater.*, 2006, **18**, 2073; (b) Y. Xia, Z. Yang and R. Mokaya, *Nanoscale*, 2010, **2**, 639; (c) A. B. Fuertes, *Chem. Mater.*, 2004, **16**, 449.
- (a) J. Wang and S. Kaskel, *J. Mater. Chem.*, 2012, **22**, 23710; (b) B. McEnaney, in *Handbook of Porous Solids*, ed. F. Schuth, K. S. W. Sing and J. Weitkamp, Wiley-VCH, Weinheim, 2002, vol. 3, pp. 1828–1863.

